

# Dual-objective optimization of organic Rankine cycle (ORC) systems using genetic algorithm: a comparison between basic and recuperative cycles

Nasir Hayat<sup>1</sup> · Muhammad Tahir Ameen<sup>1</sup>  · Muhammad Kashif Tariq<sup>1</sup> · Syed Nadeem Abbas Shah<sup>1</sup> · Ahmad Naveed<sup>1</sup>

Received: 30 June 2016 / Accepted: 7 February 2017 / Published online: 6 March 2017  
© Springer-Verlag Berlin Heidelberg 2017

**Abstract** Exploitation of low potential waste thermal energy for useful net power output can be done by manipulating organic Rankine cycle systems. In the current article dual-objectives ( $\eta_{th}$  and SIC) optimization of ORC systems [basic organic Rankine cycle (BORC) and recuperative organic Rankine cycle (RORC)] has been done using non-dominated sorting genetic algorithm (II). Seven organic compounds (R-123, R-1234ze, R-152a, R-21, R-236ea, R-245ca and R-601) have been employed in basic cycle and four dry compounds (R-123, R-236ea, R-245ca and R-601) have been employed in recuperative cycle to investigate the behaviour of two systems and compare their performance. Sensitivity analyses show that recuperation boosts the thermodynamic behaviour of systems but it also raises specific investment cost significantly. R-21, R-245ca and R-601 show attractive performance in BORC whereas R-601 and R-236ea in RORC. RORC, due to higher total investment cost and operation & maintenance costs, has longer payback periods as compared to BORC.

## List of symbols

A	Heat exchanger area (m <sup>2</sup> ), annuity (\$/year)
A <sub>f</sub>	Channel flow area (m <sup>2</sup> )
A <sub>1p</sub>	Projected area per plate (m <sup>2</sup> )
A <sub>p</sub>	Developed area per plate (m <sup>2</sup> )
b	Mean channel spacing (m)
Bo	Boiling number
BORC	Basic organic Rankine cycle

CF	Cash flow (\$/year)
CIF	Cash inflow (\$/year)
COF	Cash outflow (\$/year)
C <sub>p</sub>	Specific heat capacity (J/kg K)
CRF	Capital recovery factor
D	Port diameter (m)
EPC	Electricity production cost (\$/kWh)
f	Friction factor, operation, maintenance and insurance cost factor
G	Mass flux (kg/s m <sup>2</sup> )
GA	Genetic algorithm
GWP	Global warming potential
h	Enthalpy (J/kg), operational hours (h/year)
HPCD	Horizontal port centre distance (m)
k	Thermal conductivity (W/m K)
L	Length of plate (m)
LMTD	Log mean temperature difference (°C)
m	Mass flow rate (kg/s)
n	Plant depreciation period (years)
N <sub>p</sub>	Number of thermal plates
NPV	Net present value (\$)
Nu	Nusselt number
ODP	Ozone depletion potential
ORC	Organic rankine cycle
p	Plate pitch (m)
P <sub>co</sub>	Corrugations pitch
PHE	Plate heat exchanger
PP	Payback period (years)
PPTD	Pinch point temperature difference (°C)
Pr	Prandtl number
Q	Heat transfer (kW)
q''	Average imposed heat flux (W/m <sup>2</sup> )
Re	Reynolds number
RORC	Recuperative organic Rankine cycle
r	Discounted interest rate per annum (%)

✉ Muhammad Tahir Ameen  
tahir.ameen@uet.edu.pk

<sup>1</sup> Department of Mechanical Engineering, University of Engineering and Technology, G.T. Road, Lahore 54890, Pakistan

SIC	Specific investment cost (\$/kW)
t	Plate thickness (m), time (years)
TIC	Total investment cost (\$)
U	Overall heat transfer coefficient ( $\text{W}/\text{m}^2 \text{K}$ )
VPCD	Vertical port centre distance (m)
W	Work (kW), width of plate (m)
WHR	Waste heat recovery
$\Delta P$	Pressure drop (kPa)

### Greek letters

$\alpha$	Convective heat transfer coefficient ( $\text{W}/\text{m}^2 \text{K}$ )
$\beta$	Chevron angle ( $^\circ$ )
$\phi$	Enlargement factor
$\eta$	Thermal efficiency (%)
$P_{co}$	Corrugations pitch (m); $P_{co}$
$\mu$	Viscosity (Pa s)
$\rho$	Density ( $\text{kg}/\text{m}^3$ )

### Subscripts

acc	Acceleration
ch	Channel
cond	Condenser
e	Equivalent, effective
ele	Elevation
evap	Evaporator
f	Saturated liquid state
g	Saturated vapor state
h	Hydraulic
hs	Heat source
m	Mean
op	Operational
p	Plate, port
r	Refrigerant side
s	Isentropic
sp	Single-phase
tp	Two-phase
turb	Turbine
w	Water side
I	Preheating stage
II	Evaporation stage
III	Superheating stage
IV	Desuperheating stage
V	Condensing stage

## 1 Introduction

Knowing that how effectively low grade waste heat recovery systems can be built up by implementing characteristically low boiling point organic compounds as working fluids in organic Rankine cycle (ORC) systems, the task is to explore further and optimize linked parameters that can affect the thermodynamic and economic performance of

these innovative systems. The idea of using this technology is concrete and has been explored potentially since 1980s as an alternative technology to environmental unfriendly resources [1]. Low grade waste thermal energy is ejected as in the form of exhaust gases of combustion as well as it can be obtained from nature as in the form of geothermal form or solar irradiance. This type of energy is recorded to be more than 50% of overall heat produced in the industry [2] and therefore this abundant waste thermal energy, usually at a temperature below 200 °C requires that it be used as a viable source of environmental friendly development of sustainable systems for meeting world energy demands which are expected to rise by 53% from 2008 to 2035 [3].

As far as structure of vapor power ORC systems is concerned, basic components are same as seen in conventional steam run Rankine cycle systems [4] which are a recirculation pump, evaporator, turbine and condenser. Design optimizations to get best performance of such innovative systems require proper selection of work producing device (expander or turbine) and work consuming device (recirculating pump) together with heat exchanging devices to help carry out evaporation and condensation of working fluid during cyclic process. Related heat transfer and pressure drop characteristics of organic compounds used as working fluids are also of utmost importance. Studies show that plate type of heat exchangers (PHEs) are primarily being used and investigated because of their superior benefits over shell and tube type of heat exchangers for fulfilling evaporative and condensing needs in these sophisticated systems [5, 6]. Walraven et al. [5] optimized cycle configuration along with plate heat exchangers and shell and tube heat exchangers' optimization. Performance of plate type heat exchangers has been found better than that of shell and tube type heat exchangers for ORC systems. Jin et al. [6] highlighted the popular use of plate heat exchangers in various industries and performed computational fluid dynamics (CFD) analysis to get temperature and velocity distributions inside plates of heat exchanger. Although plate heat exchangers are superior to their counterparts but they involve variety of complex design parameters which need further investigations. Wang and Sunden [7] put forward a way of optimally designing the PHEs by including and excluding pressure drop conditions.

As a whole the performance indicators of various types associated with such systems have been studied [4, 8, 9] subjected to thermodynamic optimization. After having thermal optimization done the very next step that needs attention is to deal with economics of these systems so that they can be made cost optimized and thus attractive for commercial or domestic developers. A few researchers have also contributed in improving economics of ORC systems [10–12]. Meinel et al. [11] highlighted the thermal and economic benefits of three ORC systems by implementing

regeneration pre-heating process in basic systems. Efforts have also been made related to combined parametric optimization of systems i.e. by considering thermodynamic and economical aspects simultaneously [13–17]. Quoilin et al. [13] presented an overview of many ORC applications. Cost figures and associated technical challenges have been thoroughly discussed. Lecompte et al. [16] assessed subcritical, trilateral and transcritical cycles on thermodynamic and economic basis. The cycles were compared for three cases of heat recovery and results showed that only marginal benefit is obtained by using high temperature of the heat source. Multiobjective optimization was done to carry out thermo-economic analysis and the results were found to be attractive for ORC systems developers. In many studies [18–22] the thermo-economic analysis has been done by using multiobjective optimization method of genetic algorithm. Therefore, by considering its importance and effectiveness in optimizing complex and multivariable dependent non-linear objective functions this method has been used in this research work. In various past works it is also studied that the suggested correlations which were found for one particular organic compound have been used to determine the heat transfer and pressure drop characteristics of other organic compounds in PHEs in order to prepare results for optimization of ORC systems [19, 20]. There exists no such general theory or mathematical correlation that can cover all possible variations with respect to geometry and combinations of PHEs [23]. So in this work the necessary correlations to be used in heat exchangers designing phase are taken from extensive survey of available literature [23–27].

Furthermore different possible structures can be suitable for these systems depending upon boundary conditions [28]. Roy and Misra [29] parametrically optimized regenerative ORC system by employing R-123 and R-134a as working fluids. Imran et al. [30] investigated single stage and double stage regenerative ORC systems using five various organic compounds. The study results showed R-245ca to be best organic compound under considered conditions. Maraver et al. [31] provided optimization guidelines for subcritical, transcritical, regenerative and non-regenerative cycles. Similarly Lecompte et al. [16] worked on subcritical, trilateral and transcritical cycles. It is learnt that recuperation in ORC systems has not been given much attention in previous optimization analyses. The current research work intends to compare two architectures of ORC systems i.e. basic (BORC) and recuperative (RORC) systems with respect to thermodynamics and economics (SIC, NPV) point of view. The results have been obtained through multiobjective (dual-objective in this case) based optimization method of genetic algorithm and they significantly show how recuperation adds value to effective use of low grade waste thermal energy but at the expense of rise in system cost. Although it is difficult to develop an absolute analysis

of ORC systems because of variable boundary conditions of background processes and scenarios of technical parameters but the results are sufficient enough and aspire to provide general idea and guidelines of varied results by having modification in BORC system.

## 2 Methodology

The methodology adopted for the current research comprises of numerical modelling of two organic Rankine cycles (BORC, RORC). Dual-objective optimization has been made by selecting two conflicting objective functions which are thermal efficiency and specific investment cost (SIC). Thermal part of modelling includes process modelling as a whole and heat exchangers design in particular. The mathematical models correlate the thermodynamics and costs of the systems with the objective functions and decision variables. Numerical model has been coded in MATLAB (version R2012a) so as to use multiobjective optimization tool having fast and elitist genetic algorithm environment for optimization process. The two objectives are multivariable dependent mathematical functions. In this work four key variables, evaporation pressure, superheat and pinch temperature differences across evaporator and condenser, serve as decision variables and their operating range (upper and lower bounds) is decided subjected to defined operating simulation conditions.

Proper organic working fluids selection is itself a complete study and requires many thermodynamic, physical, heat transfer and environmental considerations before they are chosen by elimination method (involving their category, molecular complexities, critical temperatures, ODP and GWP) [32–34]. Based on investigations done in past seven suitable candidate working fluids are selected for BORC system and four of them which are dry in nature are selected for RORC system. In Table 1 thermo-physical and safety properties of various picked organic compounds are presented.

Finally, pareto optimal solutions are obtained after running optimization process and system performance is analysed thermo-economically. Two cycles are compared with each other and effect of recuperation is analysed. Sensitivity analyses has been performed to investigate the effect of variations in decision variables (i.e., evaporation pressure, superheat, pinch temperature differences across evaporator and condenser) in the investigated range. Similarly, sensitivity analysis for dimensionless Numbers (Reynolds, Prandtl, Nusselt and Boiling Numbers) with change in decision variables has also been performed.

The organic working fluids' thermodynamic and transport properties were taken by calling REFPROP version 9.0 (NIST: National Institute of Standards and

**Table 1** Thermo-physical and safety properties of organic compounds employed

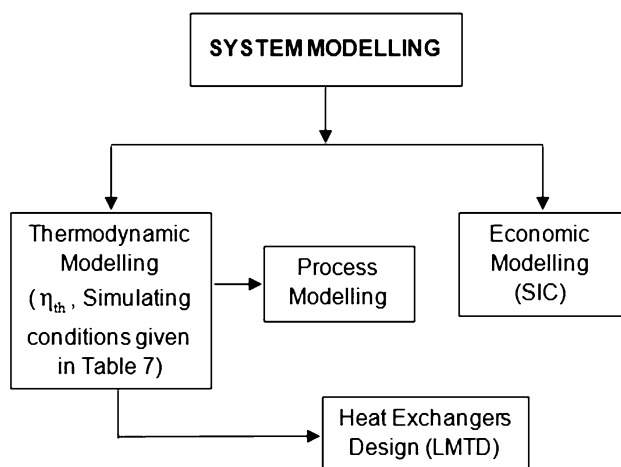
Fluid category <sup>a</sup>	ASHRAE number	ODP	GWP	Molecular mass (kg/kmol)	Boiling point (°C)	Critical temp (°C)	Critical pressure (kPa)	Safety group <sup>b</sup>
Wet	R-21	0.04	151	102.92	8.86	178.33	5181	B1
	R-152a	0	124	66.06	−24.03	113.26	4517	A2
Dry	R-123	0.012	120	152.93	27.85	183.79	3674	B1
	R-236ea	0	1370	152.04	6.18	139.29	3502	A2
	R-245ca	0	693	134.05	25.13	174.42	3925	N/A
	R-601	0	5	72.15	36.06	196.56	3370	A3
Isentropic	R-1234ze	0	6	114.04	−19.0	109.36	3636	A2L

Organic compounds are presented in order of decreasing molecular mass in specific fluid category

1: no flame propagation; 2: lower flammability; 3: higher flammability; A: lower toxicity; B: higher toxicity; 2L: lower flammability and maximum burning velocity of less than 10 cm/s; N/A: not available

<sup>a</sup> Based on slope of saturation vapor curve on T–s diagrams

<sup>b</sup> ASHRAE Standard 34—refrigerant safety group classification

**Fig. 1** Numerical modelling

Technology) using subroutines linked in the MATLAB program. Besides evaluating specific investment cost (SIC), the economic profitability and feasibility of the proposed systems have been evaluated in terms of net present value (NPV), payback period (PP) and electricity production cost (EPC) for a unit power generation.

### 3 System configuration for numerical modelling

Organic Rankine cycles (BORC, RORC), both subcritical, have been investigated and compared in the current study. Figure 1 illustrates the approach adopted for modelling of the organic Rankine cycle (ORC) systems.

Figure 2a–d shows the schematic and actual T–s diagrams of Basic ORC and Recuperative ORC. The thermodynamic cycle for BORC consists of four processes

1. Process 1s-2: Isobaric heat addition in evaporator (pre-heating, vaporization and superheating)
2. Process 2-3s: Isentropic vapor expansion in turbine
3. Process 3s-4: Isobaric heat rejection in condenser (desuperheating and condensation)
4. Process 4-1s: Isentropic compression in circulation pump

Recuperation in ORC system requires a supplementary component which is an internal heat exchanger to make use of leftover enthalpy of superheated vapors after turbine exit. The sequence of thermodynamic processes is as below

1. Process 1s-1': Isobaric preheating in recuperator
2. Process 1'-2: Isobaric heat addition in evaporator (pre-heating, vaporization and superheating)
3. Process 2-3s: Isentropic expansion in the turbine
4. Process 3s-3': Isobaric pre-desuperheating in recuperator
5. Process 3'-4: Isobaric heat rejection in condenser (desuperheating and condensation)
6. Process 4-1s: Isentropic compression in circulation pump

#### 3.1 Process thermodynamic modelling

In BORC system, the heat obtained (kW) in evaporator by the organic working fluid is

$$Q_{evap} = \dot{m}_r(h_2 - h_1) \quad (1)$$

In RORC system similar heat gain (kW) is

$$Q_{evap} = \dot{m}_r(h_2 - h_{1'}) \quad (1a)$$

The turbine work (kW) produced during vapor expansion is

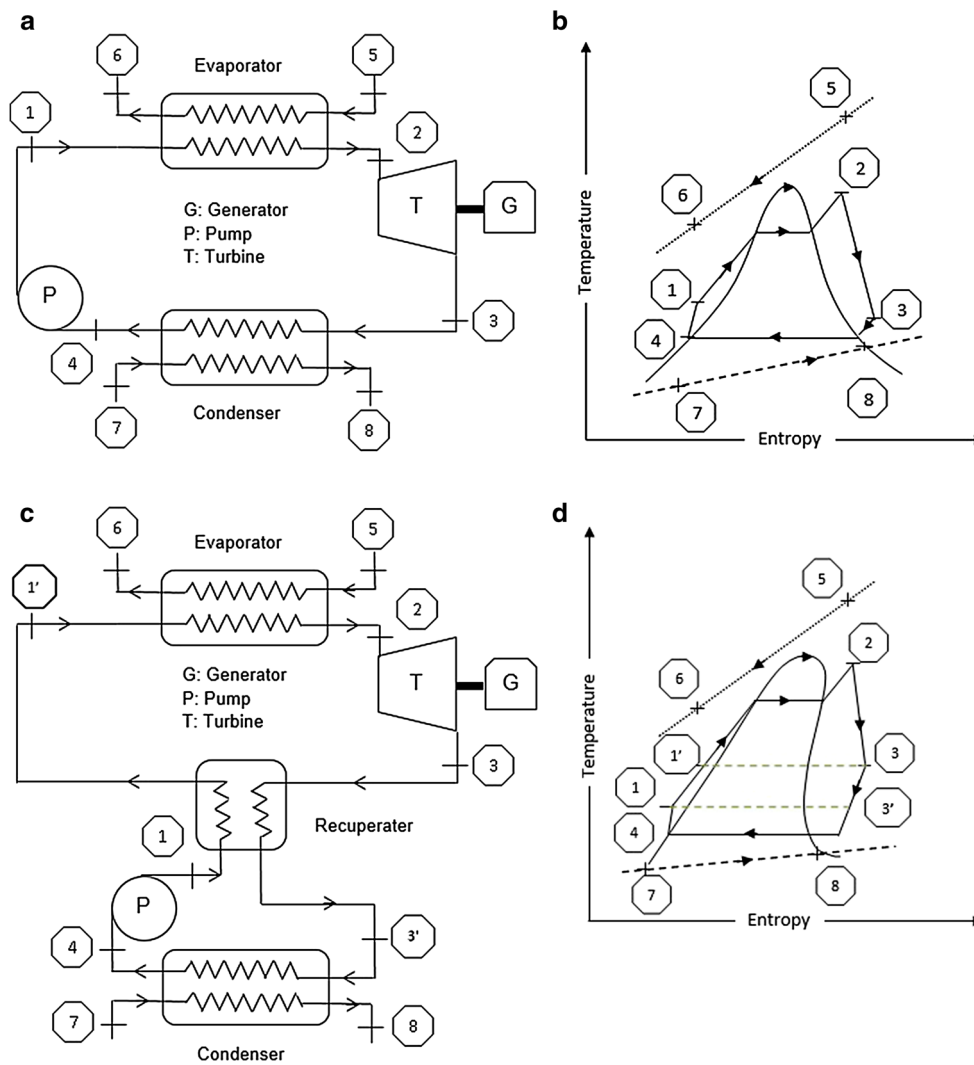


**Fig. 2** a The schematic of BORC. b The T–s diagram of BORC. c The schematic of RORC. d The T–s diagram of RORC

$$W_{turb} = \dot{m}_r \eta_{turb} (h_2 - h_{3s}) \tag{2}$$

Heat rejected (kW) by the working fluid in the vapor condenser is

$$Q_{cond} = \dot{m}_r (h_3 - h_4) \tag{3}$$

Work required by pump (kW) is

$$W_{pump} = \frac{\dot{m}_r (h_{1s} - h_4)}{\eta_{pump}} \tag{4}$$

The thermal efficiency for any ORC system is the ratio of net useful work obtained to the heat input given in evaporator

$$\eta_{th} = \frac{(W_{turb} - W_{pump})}{Q_{evap}} \tag{5}$$

### 3.2 Heat exchanger’s design

Evaporator and condenser heat exchangers are chevron type plate heat exchangers (PHEs). They are compact and depict better thermodynamic and hydraulic performances over equivalent shell and tube type counterparts [5, 7]. However, PHE provides higher pressure drops because of increased turbulence due to corrugated geometry so for design objective allowable pressure drops have to be set to a threshold value of 5% of inlet pressure of fluids. As far as type of recuperator heat exchanger is concerned, its selection as a PHE is made due to the reason that recuperative architectures of ORC systems are designed without extracting any fraction of superheated vapors during turbine stages rather the left over superheated vapors after turbine exit are given the chance of transferring their thermal potential to subcooled liquid after pump

exit (Fig. 2c). In the former case feed-heaters are utilized which are usually direct contact mixing heat exchangers. They involve heat transfer as well as mass transfer and normally use feed pumps additionally [30, 35–37]. On the contrary in the latter case literature is limited and does not highlight specific type of heat exchanger construction wise for reclaiming the heat. In few research works optimizations have been run without identifying type of heat exchanger [29, 38–40]. There exists use of closed surface type of heat exchangers such as shell and tube type [15, 41] and plate type [14, 42, 43] for recuperation. Therefore, in present work making use of similar PHE because of its benefits over shell and tube type counterpart a feasibility check is developed and results are compared without and with implementing recuperator (see Sect. 5).

Turbine and pump are designed conditionally with their thermodynamic efficiencies of 75 and 65% respectively [30]. All heat exchangers are modelled on the basis of LMTD method having steady state counter current flow conditions established (see Fig. 3a, b). Heat exchangers are built of stainless steel AISI-304 material [6, 44]. Secant method based iteration procedure is employed in algorithm to evaluate unique value of number of thermal plates  $N_p$  which satisfies the heat transfer surface area requirement proposed by the energy balance condition. The design evaluation starts by proposing a suitable geometry of heat exchanger prematurely.

Few assumptions are necessarily defined in regard of working with PHEs which include having steady state environment, fully developed flow in corrugated plate channels, negligible heat lost to surroundings and negligible fouling effects [20]. Moreover all fluid properties for heat carrier source, working fluid and cooling source sides are calculated by using average of the bulk temperatures at respective inlet and outlet state points [20].

### 3.2.1 Geometry parameters of PHEs

The basic geometry of a PHE is illustrated in Fig. 4 and the defined values for parameters are presented in Table 2. Relationships of geometrical parameters of critical importance are given below.

Depending on overall dimensions the total area of a PHE is related as

$$A_{total} = (N_p - 2)A_p \quad (6)$$

Here area of single plate is expressed as

$$A_p = L_e W_e \quad (7)$$

Here  $L_e$  and  $W_e$  are effective length and width of a PHE. Chevron angle ( $\beta$ ) is measure of softness or hardness of thermal and hydraulic characteristics of plates. Difference between plate pitch and plate thickness is termed as mean channel spacing ( $b$ ). Mean channel spacing and corrugation pitch based ratio of developed area to projected area of one plate of PHE [19] expressed as surface enlargement factor is

$$\Phi = \frac{1}{6} \left[ 1 + \left\{ \sqrt{1 + \left( \frac{b\pi}{P_{co}} \right)^2} \right\} + 4 \sqrt{1 + \frac{\left( \frac{b\pi}{P_{co}} \right)^2}{2}} \right] \quad (8)$$

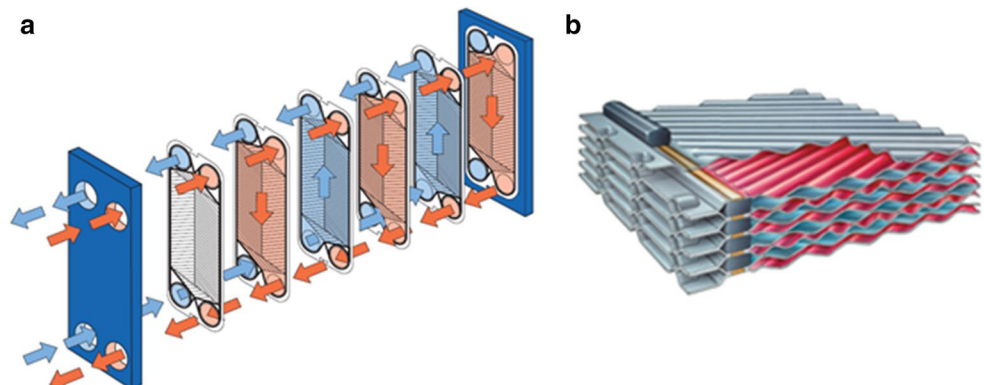
Channel flow area which is the minimum flow area between plates and is obtained as a product of mean channel spacing and width of plate is

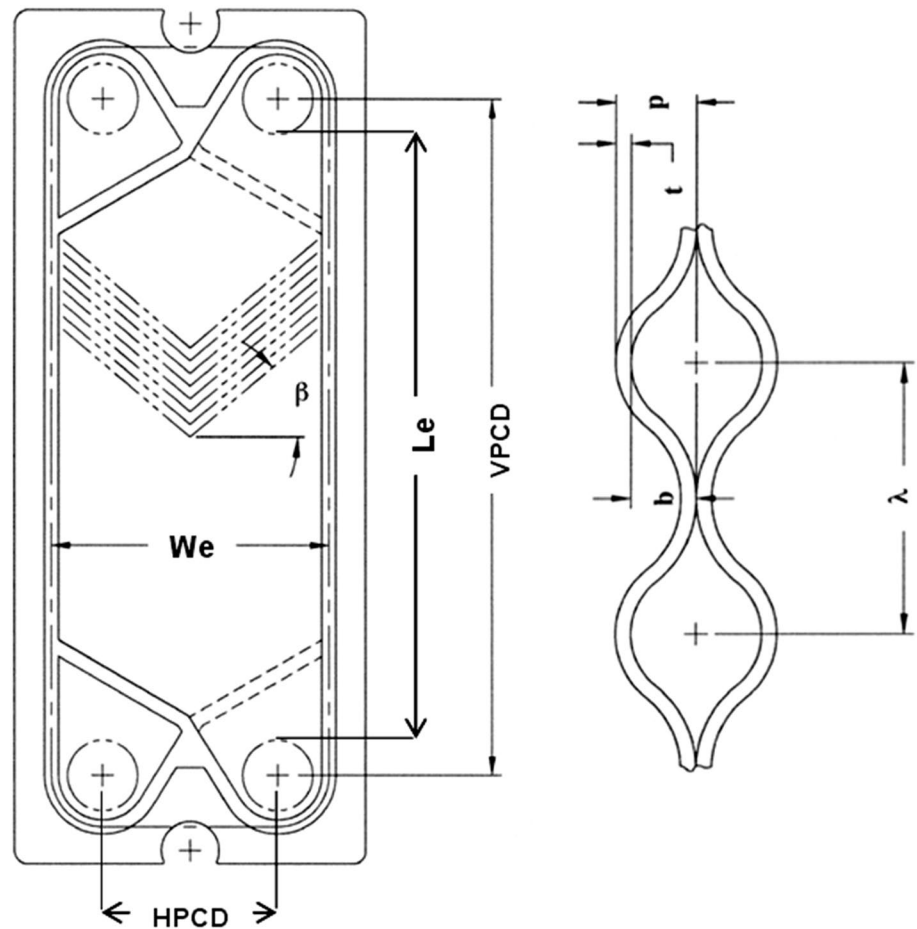
$$A_f = bW_e \quad (9)$$

Four times ratio of channel flow area to wetted perimeter gives hydraulic diameter while equivalent diameter is approximated as twice of place spacing

$$D_h \cong \frac{2b}{\Phi} \quad \text{when } b \ll W_e \quad (10)$$

**Fig. 3** **a** Flow pattern inside PHE. **b** Corrugated channels



**Fig. 4** Basic geometry of a plate heat exchanger (PHE) [25]**Table 2** Parameters defining the geometry of PHEs

Parameter	Designation (units)	Design values for		
		Evaporator	Condenser	Recuperator
Vertical port center distance	VPCD (m)	1.45	1.5	0.975
Horizontal port center distance	HPCD (m)	0.35	0.3	0.285
Effective width	$W_e$ (m)	0.55	0.55	0.385
Effective length	$L_e$ (m)	1.25	1.25	0.875
Plate pitch	$p$ (m)	0.0035	0.0045	0.0035
Plate thickness	$t$ (m)	0.0005	0.0005	0.0005
Mean channel spacing	$b$ (m)	0.003	0.004	0.003
Channel flow area	$A_f$ (m <sup>2</sup> )	0.00165	0.0022	0.001155
Corrugation pitch	$P_{co}$ (m)	0.01	0.013	0.01
Projected area per plate	$A_{1p}$ (m <sup>2</sup> )	0.6875	0.6875	0.3369
Enlargement factor	$\Phi$	1.1968	1.1968	1.1968
Developed area per plate	$A_p$ (m <sup>2</sup> )	0.8228	0.8228	0.4032
Hydraulic diameter	$D_h$ (m)	0.005	0.0067	0.005
Chevron angle	$\beta$ (°)	60	60	60

$$D_e \cong 2b \tag{11}$$

### 3.3 Thermodynamic modelling

Thermodynamic modelling of heat exchanging components include determination of compulsory heat exchanging area requirements from heat balance keeping allowable pressure drop condition satisfied. The evaporator and condenser include single-phase and two-phase heat transfers so they can be split into separate sections or zones. Each section or zone has its own particular number of thermal plates, heat transfer area, corresponding heat transfer coefficients and pressure drops. In RORC system there is one zone only because it requires single-phase heat transfer between superheated vapors and subcooled liquid (in Fig. 2d given as 1-1'-3-3').

#### 3.3.1 Evaporator design

Superheating is considered mandatory so there will be three sections present in evaporator PHE which are single-phase preheating (I), two-phase vaporization (II) and single-phase superheating (III) as symbolized in Fig. 5. The total area required by evaporator PHE is the sum of individual areas

$$A_{evap} = A_{sp,I} + A_{tp,II} + A_{sp,III} \tag{12}$$

The overall pressure drop equals the sum of individual pressure drops in all three sections

$$\Delta P_{evap} = \Delta P_{sf,I} + \Delta P_{tf,II} + \Delta P_{sf,III} \tag{13}$$

#### 3.3.2 Condenser design

Considering no subcooling there will be two sections in condenser which are single-phase desuperheating (IV) and two-phase condensing (V). The total area is

$$A_{cond} = A_{sp,IV} + A_{tp,V} \tag{14}$$

The overall pressure drop is

$$\Delta P_{cond} = \Delta P_{sf,IV} + \Delta P_{tf,V} \tag{15}$$

#### 3.3.3 Recuperator design

The only section defined in recuperator PHE is termed as single-phase recuperation (VI)

$$A_{recu} = A_{sp,VI} \tag{16}$$

The overall pressure drop is

$$\Delta P_{recu} = \Delta P_{sf,VI} \tag{17}$$

#### 3.3.4 Characteristics of single-phase sections

Preheating (I), superheating (III), desuperheating (IV) and recuperation (VI) are single-phase sections. Heat exchange in a single-phase section is

$$Q_{sp} = U_{sp} A_{sp} LMTD_{sp} \tag{18}$$

This is an implicit equation where  $A_{sp}$  is unknown and other variables are given by available simulating and heat balance conditions. Log mean temperature difference is

$$LMTD_{sp} = \frac{\Delta T_{max} - \Delta T_{min}}{\log \left( \frac{\Delta T_{max}}{\Delta T_{min}} \right)} \tag{19}$$

The overall heat transfer coefficient is

$$\frac{1}{U_{sp}} = \frac{1}{\alpha_w} + \frac{t_p}{k_p} + \frac{1}{\alpha_{r,sp}} \tag{20}$$

The Nusselt No. correlation [24] for single-phase water side heat source is

$$Nu_w = 0.724 \left( \frac{6\beta}{\pi} \right)^{0.646} Re^{0.583} Pr^{0.33} \tag{21}$$

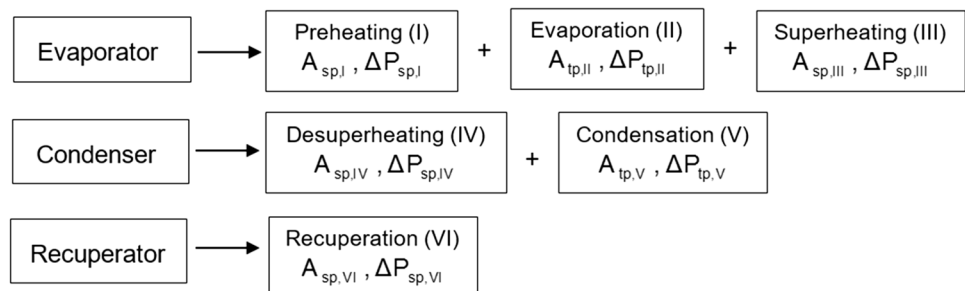
The Reynolds No. of fluid flowing in channel is

$$Re = \frac{GD_h}{\mu} \tag{22}$$

Here G is channel mass flux presented as

$$G = \frac{\dot{m}}{N_{ch} b W_e} \tag{23}$$

**Fig. 5** Zones in all heat exchangers





The Prandtl No. is

$$\text{Pr} = \frac{C_p \mu}{k} \quad (24)$$

The convective heat transfer coefficient is

$$\alpha_w = \frac{Nu_w k_w}{D_h} \quad (25)$$

The Nusselt No. correlation [25] for single-phase refrigerant side is

$$Nu_{r,sp} = 0.2092 \text{Re}^{0.78} \text{Pr}^{0.33} \left( \frac{\mu_m}{\mu_{wall}} \right)^{0.14} \quad (26)$$

The convective heat transfer coefficient is

$$\alpha_{r,sp} = \frac{Nu_{r,sp} k_r}{D_h} \quad (27)$$

By neglecting other pressure drop components and considering only frictional pressure drop for opposite side fluids, the analysis is rather simplified.

$$\Delta P_f = \frac{4f_{sp} N_{ch} G^2 L_e}{2\rho D_h} \quad (28)$$

The frictional pressure drop for both heat carrier and heat receiver sides is correlated as [23]

$$f_{sp} = \frac{0.572}{\text{Re}^{0.217}} \text{ for } \text{Re} > 550 \quad (29)$$

### 3.3.5 Characteristics of two-phase sections

There are two two-phase sections encountered which are evaporation (II) and condensation (V). Heat exchange in any two-phase section is

$$Q_{tp} = U_{tp} A_{tp} \text{LMTD}_{tp} \quad (30)$$

The Log Mean Temperature Difference is

$$\text{LMTD}_{tp} = \frac{\Delta T_{\max} - \Delta T_{\min}}{\log \left( \frac{\Delta T_{\max}}{\Delta T_{\min}} \right)} \quad (31)$$

The overall heat transfer coefficient is

$$\frac{1}{U_{tp}} = \frac{1}{\alpha_w} + \frac{t_p}{k_p} + \frac{1}{\alpha_{r,tp}} \quad (32)$$

For both evaporation and condensation, the Nusselt No. and associated heat transfer coefficients for heat carrier and cooling water sides are given from Eqs. (21) and (25). For refrigerant side the Nusselt No. correlation [27] in evaporation in a vertical type PHE is

$$Nu_{r,tp,II} = Ge_1 \text{Re}_{eq}^{Ge_2} Bo_{eq}^{0.3} \text{Pr}^{0.4} \quad (33)$$

$$Ge_1 = 2.81 \left( \frac{P_{co}}{D_h} \right)^{-0.041} \left( \frac{\pi}{2} - \beta \right)^{-2.83} \quad (34)$$

$$Ge_2 = 0.746 \left( \frac{P_{co}}{D_h} \right)^{-0.082} \left( \frac{\pi}{2} - \beta \right)^{0.61} \quad (35)$$

$$\text{Re}_{eq} = \frac{G_{eq} D_h}{\mu_f} \quad (36)$$

$$G_{eq} = G \left[ (1-x) + x \left( \frac{\rho_f}{\rho_g} \right)^{0.5} \right] \quad (37)$$

$$Bo_{eq} = \frac{q''}{G_{eq} i_{fg}} \quad (38)$$

For refrigerant the Nusselt No. correlation [26] during condensation in a vertical PHE is

$$Nu_{r,tp,V} = Ge_5 \text{Re}_{eq}^{Ge_6} \text{Pr}^{0.33} \quad (39)$$

$$Ge_5 = 11.22 \left( \frac{P_{co}}{D_h} \right)^{-0.283} \left( \frac{\pi}{2} - \beta \right)^{-4.5} \quad (40)$$

$$Ge_6 = 0.35 \left( \frac{P_{co}}{D_h} \right)^{0.23} \left( \frac{\pi}{2} - \beta \right)^{1.48} \quad (41)$$

Corresponding convective heat transfer coefficients can be obtained by using Eq. (27). As a whole four components are summed up together to give total pressure drop in two-phase sections. These are pressure drop due to acceleration of the working fluid, pressure drop due to elevation change because of height of PHE, pressure drop due to inlet and exit fluid ports and most importantly pressure drop due to the friction of flowing fluid inside the heat exchangers.

In evaporation the two-phase friction factor is expressed by [27]

$$f_{tp,II} = Ge_3 \text{Re}_{eq}^{Ge_4} \quad (42)$$

$$Ge_3 = 64710 \left( \frac{P_{co}}{D_h} \right)^{-5.27} \left( \frac{\pi}{2} - \beta \right)^{-3.03} \quad (43)$$

$$Ge_4 = -1.314 \left( \frac{P_{co}}{D_h} \right)^{-0.62} \left( \frac{\pi}{2} - \beta \right)^{-0.47} \quad (44)$$

In condensation the two-phase friction factor is given by [26]

$$f_{tp,V} = Ge_7 \text{Re}_{eq}^{Ge_8} \quad (45)$$

$$Ge_7 = 3521.1 \left( \frac{P_{co}}{D_h} \right)^{4.17} \left( \frac{\pi}{2} - \beta \right)^{-7.75} \quad (46)$$

$$Ge_8 = -1.024 \left( \frac{P_{co}}{D_h} \right)^{0.0925} \left( \frac{\pi}{2} - \beta \right)^{-1.3} \quad (47)$$

In above mentioned mathematical relations the constants from  $Ge_1$  to  $Ge_8$  are non-dimensional geometric parameters which rely upon PHE’s geometrical parameters such as hydraulic diameter ( $D_h$ ), corrugation pitch ( $P_{co}$ ) and chevron angle ( $\beta$ ) [27].

Frictional pressure drop is

$$\Delta P_f = \frac{4f_{tp}N_{ch}G^2L_e}{2\rho D_h} \quad (48)$$

The acceleration pressure drop is

$$\Delta P_{acc} = G_{eq}^2 x (v_g - v_f) \quad (49)$$

Here  $G_{eq}$  is the equivalent mass flux

$$G_{eq} = \frac{\dot{m}_{eq}}{bN_{ch}W_p} \quad (50)$$

The equivalent mass flow is

$$\dot{m}_{eq} = \dot{m} \left[ (1-x) + x \left( \frac{\rho_f}{\rho_g} \right)^{0.5} \right] \quad (51)$$

The change in pressure due to elevation positive upward is

$$\Delta P_{ele} = g\rho_m L_e \quad (52)$$

Mean density is

$$\frac{1}{\rho_m} = \left( \frac{x}{\rho_g} + \frac{1-x}{\rho_f} \right) \quad (53)$$

The port pressure drop for inlet and outlet manifolds is

$$\Delta P_p = 1.4 \frac{G_p^2}{\rho_m} \quad (54)$$

Port mass flux is

Fig. 6 Heat exchanger sizing

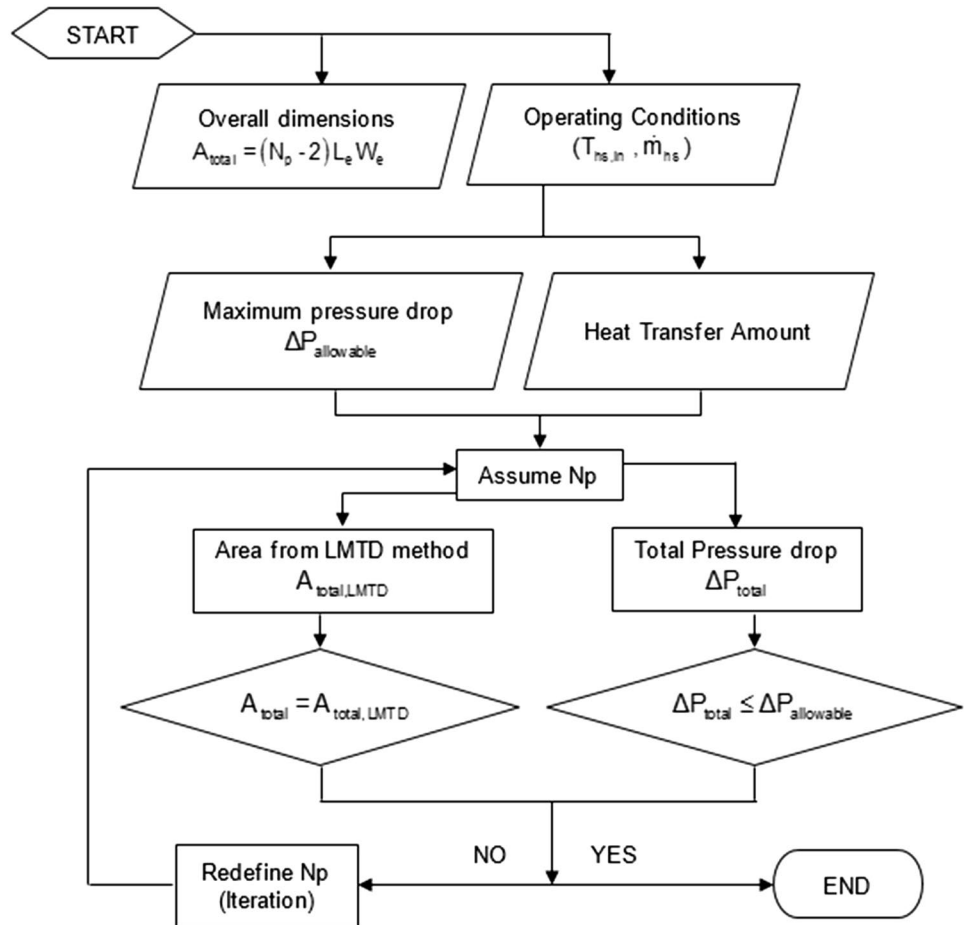


**Table 3** Cost constants of integral components of ORC systems

Heat exchangers		Turbine		Pump	
Constant	Value	Constant	Value	Constant	Value
$F_s$	1.70	$F_s$	1.70	$F_s$	1.70
$F_{M,HX}$	2.40	$F_{MP,TR}$	3.50	$F_{M,PP}$	2.20
$K_{1,HX}$	4.66	$K_{1,TR}$	2.2659	$K_{1,PP}$	3.3890
$K_{2,HX}$	-0.1557	$K_{2,TR}$	1.4398	$K_{2,PP}$	0.5360
$K_{3,HX}$	0.1547	$K_{3,TR}$	-0.1776	$K_{3,PP}$	0.1538
$B_{1,HX}$	0.96			$B_{1,PP}$	1.89
$B_{2,HX}$	1.21			$B_{2,PP}$	1.35
$C_{1,HX}$	0.00			$C_{1,PP}$	-0.3935
$C_{2,HX}$	0.00			$C_{2,PP}$	0.3957
$C_{3,HX}$	0.00			$C_{3,PP}$	-0.00226

$$G_p = \frac{\dot{m}_{eq}}{\left(\frac{\pi D_p^2}{4}\right)} \tag{55}$$

The two-phase total pressure drop is

$$\Delta P_{tp} = \Delta P_f + \Delta P_{acc} + \Delta P_{ele} + \Delta P_p \tag{56}$$

The layout plan for design of a heat exchanger is given here in Fig. 6.

### 3.4 Economic modelling of system

#### 3.4.1 Components cost

Chemical Engineering Plant Cost Index (CEPCI) has been used (year 2013) to obtain the costs of all integral components of the system. Atrens et al. [12] studied cost estimation regarding CO<sub>2</sub> based Enhanced Geothermal System (EGS) plant. The similar technique was also applied by other researchers in their works [14, 20]. The same approach is implemented here to get the costs of all individual key components of the system.

Cost for evaporator, condenser and recuperator PHEs is found by using similar relation in which constants essentially depend upon the equipment type (heat exchanger).

$$Cost_{HX} = \frac{527.7}{397} (B_{1,HX} + B_{2,HX} F_{M,HX} F_{P,HX}) F_s C_{b,HX} \tag{57}$$

Here  $B_{1,HX}$  and  $B_{2,HX}$  are constants for particular type of heat exchanger.  $F_{M,HX}$  is steel (SS) material factor.  $F_{P,HX}$  is pressure factor of heat exchanger and is determined as

$$\log(F_{P,HX}) = C_{1,HX} + C_{2,HX} \log(P_{HX}) + C_{3,HX} \log(P_{HX})^2 \tag{58}$$

Here  $C_{1,HX}$ ,  $C_{2,HX}$  and  $C_{3,HX}$  are the constants based upon heat exchanger type.  $P_{HX}$  is design pressure of heat

exchanger. In Eq. (57),  $F_s$  is the additional factor related to running and fixing costs for material, piping, labour and other extras.  $C_{b,HX}$  is the basic cost whose calculation is governed by heat transfer area and few constants as follows

$$\log(C_{b,HX}) = K_{1,HX} + K_{2,HX} \log(A_{HX}) + K_{3,HX} (\log(A_{HX}))^2 \tag{59}$$

$K_{1,HX}$ ,  $K_{2,HX}$  and  $K_{3,HX}$  are the constants for heat exchanger type.  $A_{HX}$  is required area of heat exchanger (m<sup>2</sup>). Turbine is made up of SS and its cost is given by

$$Cost_{TR} = \frac{527.7}{397} (F_{MP,TR} F_s C_{b,TR}) \tag{60}$$

$F_{MP,TR}$  is combine material and pressure factor for the turbine material of steel. Basic cost of steel turbine is as follows

$$\log(C_{b,TR}) = K_{1,TR} + K_{2,TR} \log(W_{turb}) + K_{3,TR} (\log(W_{turb}))^2 \tag{61}$$

Here  $K_{1,TR}$ ,  $K_{2,TR}$  and  $K_{3,TR}$  are constants specifically for turbine.  $W_{turb}$  is turbine power output (kW) calculated from Eq. (2). Centrifugal type of pump is used made of carbon steel material. Pump cost is expressed as

$$Cost_{PP} = \frac{527.7}{397} (B_{1,PP} + B_{2,PP} F_{M,PP} F_{P,PP}) F_s C_{b,PP} \tag{62}$$

$B_{1,PP}$  and  $B_{2,PP}$  are constants for type of pump which is centrifugal.  $F_{M,PP}$  is the material factor and pressure factor  $F_{P,PP}$  is

$$\log(F_{P,PP}) = C_{1,PP} + C_{2,PP} \log(P_{PP}) + C_{3,PP} \log(P_{PP})^2 \tag{63}$$

$C_{1,PP}$ ,  $C_{2,PP}$  and  $C_{3,PP}$  are constants for centrifugal type of pump.  $P_{PP}$  is the design pressure (bar) for which pump is designed. Basic cost of pump  $C_{b,PP}$  is

$$\log(C_{b,PP}) = K_{1,PP} + K_{2,PP} \log(W_{pump}) + K_{3,PP} (\log(W_{pump}))^2 \tag{64}$$

$K_{1,PP}$ ,  $K_{2,PP}$  and  $K_{3,PP}$  are constants of pump type.  $W_{pump}$  denotes the power consumed by the pump (kW) and is

**Table 4** Typical assumed economic factors and indices [43, 45]

Parameters	Value
Discounted interest rate per annum (r)	3, 5 and 7 (%)
Plant depreciation lifetime (n)	10, 15 and 20 (years)
Plant operational hours (load occupancy) (h <sub>op</sub> )	7500 (h/year)
Operation, maintenance and insurance cost factor (f)	1.65 (%)
Salvage value	0

given by Eq. 4. The cost constants are enlisted in Table 3 for three heat exchangers, a turbine and a pump.

3.4.2 Net present value (NPV) and electricity production cost (EPC)

Net present value (NPV) and electricity production cost (EPC) are used to evaluate the feasibility/profitability after optimization for a comparable organic fluid results [43, 45–47]. Typical economic factors and indices needed are in Table 4.

The coefficient that correlates future cash flows with a present value is given by [47]

$$CF_{n=0} = \frac{CF_{n=t}}{(1+r)^n} \tag{65}$$

The net present value (NPV) is defined as to be the present value of total cash flows (both in and out) during the economic lifetime of a system [47] given as

$$NPV = CIF_{t=0} - COF_{t=0} = \sum_{j=0}^n \frac{CIF_{t=j}}{(1+r)^j} - \sum_{j=0}^n \frac{COF_{t=j}}{(1+r)^j} \tag{66}$$

Payback period (PP) is the time-period in years required by the NPV to get to zero value and is obtained by solving Eq. (66) such that NPV = 0 \$ [47]

$$\sum_{j=0}^{PP} \frac{CIF_{t=j}}{(1+r)^j} = \sum_{j=0}^{PP} \frac{COF_{t=j}}{(1+r)^j} \tag{67}$$

The annual cash generated by the investment called as annuity of the investment (A) [45, 46] is calculated by multiplying total investment cost (TIC) with capital recovery factor (CRF) presented in Eqs. (68) and (69) respectively as

$$A = TIC.CRF \tag{68}$$

$$CRF = \left[ \frac{r(1+r)^n}{(1+r)^n - 1} \right] \tag{69}$$

In the end electricity production cost (EPC) is estimated determined by [43, 45, 47] as below

$$EPC = \left[ \frac{A + f.TIC}{W_{net}.h_{op}} \right] \tag{70}$$

4 Objective functions, decision variables and bounds

The multi-objective function consisting of two conflicting objectives  $f_1(x)$  and  $f_2(x)$  is

$$F(x) = [f_1(x), f_2(x)] \quad \text{where } x = \left\{ \begin{matrix} P_{evap} \\ Superheat \\ PPTD_{evap} \\ PPTD_{cond} \end{matrix} \right\} \text{ subjected to } l.b \leq x \leq u.b$$

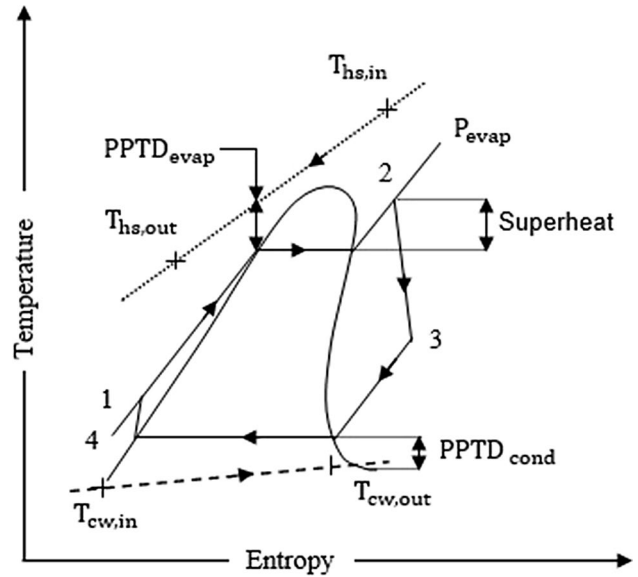


Fig. 7 Four decision variables on T–s diagram

For BORC system it is expressed as

$$F(x) = \left\{ \begin{matrix} f_1(x) = \frac{\eta_{turb}(h_2-h_3) - \frac{(h_1-h_4)}{\eta_{pump}}}{(h_2-h_1)} \\ f_2(x) = \frac{\eta_{turb}(h_2-h_3) - \frac{(h_1-h_4)}{\eta_{pump}}}{(Cost_{HX, evap} + Cost_{TR} + Cost_{HX, cond} + Cost_{PP})} \end{matrix} \right\} \tag{71}$$

For RORC system the function is

$$F(x) = \left\{ \begin{matrix} f_1(x) = \frac{\eta_{turb}(h_2-h_3) - \frac{(h_1-h_4)}{\eta_{pump}}}{(h_2-h_1)} \\ f_2(x) = \frac{\eta_{turb}(h_2-h_3) - \frac{(h_1-h_4)}{\eta_{pump}}}{(Cost_{HX, evap} + Cost_{TR} + Cost_{HX, cond} + Cost_{PP} + Cost_{HX, recu})} \end{matrix} \right\} \tag{72}$$

$f_1(x)$  is the thermal efficiency function and  $f_2(x)$  is the specific investment cost (SIC) function to be maximized and minimized respectively.

$$x = \left\{ \begin{matrix} P_{evap} \\ Superheat \\ PPTD_{evap} \\ PPTD_{cond} \end{matrix} \right\} \text{ are the decision variables which}$$

influence thermal efficiency and system cost greatly. Pinch point is the minimum temperature difference between opposite fluids in heat exchangers. The decision variables are shown on the T–s diagram in Fig. 7.

The bounds set for decision variables for optimization strictly depend upon not only each other but also predefined simulation parameters (heat source inlet temperature, critical temperature of working fluid and condensing temperature in condenser). In this section a mechanism is described for selection of bounds. Superheat bounds are independently chosen ( $0 \leq \text{Superheat} \leq 10$ ). For a working fluid the maximum saturation temperature in evaporator  $T_{\text{evap}}$  is always some degrees lesser than heat source inlet temperature  $T_{\text{hs,in}}$ . For heat transfer to take place in right direction the sum of evaporation temperature and PPTD across evaporator must be less than heat source inlet temperature and critical temperature of working fluid i.e.  $T_{\text{evap}} + \text{PPTD}_{\text{evap}} < T_{\text{hs,in}}$  and  $T_{\text{evap}} + \text{PPTD}_{\text{evap}} < T_{\text{critical}}$ . Also evaporation temperature together with superheat at turbine inlet must be less than heat source inlet temperature  $T_{\text{evap}} + \text{Superheat} < T_{\text{hs,in}}$ . These criteria decide the upper bound for evaporation pressure. Whereas lower bound for evaporation pressure is governed by condensing temperature  $T_{\text{cond}}$  which is fixed at  $30^\circ\text{C}$  for current study ( $T_{\text{evap}} > T_{\text{cond}}$ ). Past investigations show only one set of upper and lower bounds of evaporation pressure for all organic compounds and only one upper and lower bound means that it would have been selected by observing the minimum critical temperature of all available organic compounds along with other parameters. But if done this way the available potential of having higher upper limit present in other organic compounds

cannot be completely utilized. Moreover, waste heat resources are usually of low grade and demand full usage of available potential precisely. In the current study each working fluid is given its own bounds for evaporation pressure by keeping its critical temperature, heat source temperature, maximum pinch point, superheat and condensing temperature in mind. With upper limit of superheat independently set at  $10^\circ\text{C}$  the evaporation pressure must be lower than a pressure which has corresponding saturation temperature  $10^\circ\text{C}$  less than heat source inlet temperature. Similarly, with upper limit of evaporator pinch point set at  $25^\circ\text{C}$  the evaporation pressure must be lower than a pressure which has corresponding saturation temperature  $25^\circ\text{C}$  less than heat source inlet temperature. A minimum of  $6^\circ\text{C}$  of pinch point necessitate effective heat transfer between opposite fluids in heat exchangers. Upper limit for pinch point across condenser depends upon cooling water inlet temperature and condensing temperature  $T_{\text{cw,in}} + \text{PPTD}_{\text{cond}} < T_{\text{cond}}$ . This condition gives upper bound for condenser pinch point of  $15^\circ\text{C}$ . Having different evaporation pressure bounds for different fluids for same waste heat input conditions allow more search space availability for the genetic algorithm to look for an optimal solution by exploiting the available potential. If the evaporation pressure bounds are kept same then superheat or PPTD across evaporator can have separate bounds for all compounds. Table 5 summarizes the logical bounds.

**Table 5** Logical bounds for four decision variables

Organic fluid	$P_{\text{evap}}$ (kPa)		Superheat ( $^\circ\text{C}$ )		$\text{PPTD}_{\text{evap}}$ ( $^\circ\text{C}$ )		$\text{PPTD}_{\text{cond}}$ ( $^\circ\text{C}$ )	
	l.b. <sup>a</sup>	u.b. <sup>b</sup>	l.b.	u.b.	l.b.	u.b.	l.b.	u.b.
R-21	215	2155	0	10	6	25	6	15
R-152a	690	2775						
R-123	110	1320						
R-236ea	245	2105						
R-245ca	122	1585						
R-601	83	1000						
R-1234ze	580	2200						

<sup>a</sup> Lower bound

<sup>b</sup> Upper bound

**Table 6** Controlling parameters of NSGA-II (genetic algorithm)

Selection function	Tournament	Mutation function	Uniform
Population size	100	Mutation rate	0.06
Stopping criterion/generations limit	80	Pareto front fraction	0.35
Crossover fraction	0.7	Plot functions	Pareto front

**Table 7** Parameters for simulation

Parameter	Value	Parameter	Value
Heat source inlet temperature	150 °C	Condensing temperature	30 °C
Heat source mass flow rate	7 kg/s	Turbine thermal efficiency	75%
Cooling water inlet temperature	15 °C	Pump thermal efficiency	65%
Ambient conditions	Standard temperature and pressure (STP)		

**Table 8** Decision points obtained after a trade-off for BORC system

Organic fluid	Objective functions		Tradeoff SIC/ $\eta_{th}$	Decision variables				Net power (kW)
	$\eta_{th}$ (%)	SIC (\$/kW)		$P_{evap}$ (kPa)	Superheat (°C)	PPTD <sub>evap</sub> (°C)	PPTD <sub>cond</sub> (°C)	
R-21	12.6824	6418.24	506.07	1541.93	0.9438	6.4969	14.6392	201.59
R-152a	9.3424	6086.97	651.54	2765.03	0.9647	8.9489	14.8173	242.29
R-123	12.3744	6374.03	515.10	934.84	0.5304	6.5896	14.6080	211.85
R-236ea	11.4180	6068.80	531.51	2003.69	0.1737	6.8337	14.8542	235.77
R-245ca	12.0994	6063.91	501.17	1136.71	0.3909	7.0483	14.8882	215.35
R-601	12.2368	6071.83	496.19	722.37	0.1071	7.0369	14.5856	207.20
R-1234ze	8.5916	6465.64	752.55	2187.47	0.9871	12.7435	14.8016	237.69

#### 4.1 NSGA-II in genetic algorithm and Parameters

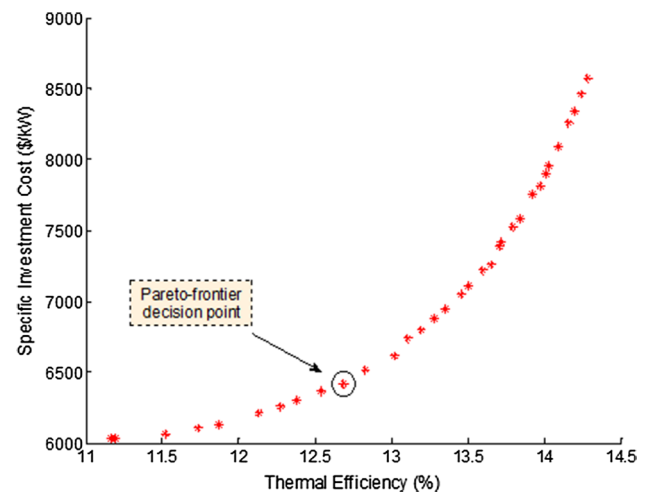
NSGA-II is a multi-objective optimization method based on genetic algorithm and features a fast sorting and elitist preservation mechanism. After each step selection of individuals is made using random number generator scheme from existing population called parents. The selected individuals are called offsprings to be used in upcoming generation. Successive generations evolve the population for an optimal solution. As genetic algorithm can be used to optimize a problem having more than one objectives at a time, the objectives need to be traded off in some way depending upon the relative importance. All optimization studies that include genetic algorithm have explained its working mechanism quite comprehensively so more details can be found in literature [20]. Table 6 defines the parameters of NSGA-II employed during current work.

For simulation purposes a few parameters have been fixed defined by the available conditions of background process mentioned in Table 7.

## 5 Results and discussion

### 5.1 Optimization results

For the investigated refrigerants, the optimization results show that thermal efficiency varies from 8.59% (R-1234ze; Isentropic) to 12.68% (R-21; Wet) whereas SIC varies from

**Fig. 8** Pareto optima for R-21

6063.91 \$/kW (R-245ca; Dry) to 6465.64 \$/kW (R-1234ze; Isentropic). Table 8 summarizes the results for all working fluids with net power output.

It is evident from the results that there exists no single working fluid which has highest thermal efficiency in tandem with the minimum SIC. This necessitates the trade-off i.e. pareto optima. Figure 8 shows the pareto optima for best performing working fluid (R-21) in BORC system.

The Pareto front obtained from genetic algorithm for RORC system is shown in Fig. 9 for one best performing dry compound (R-601). Table 9 summarizes the results obtained for all dry compounds.

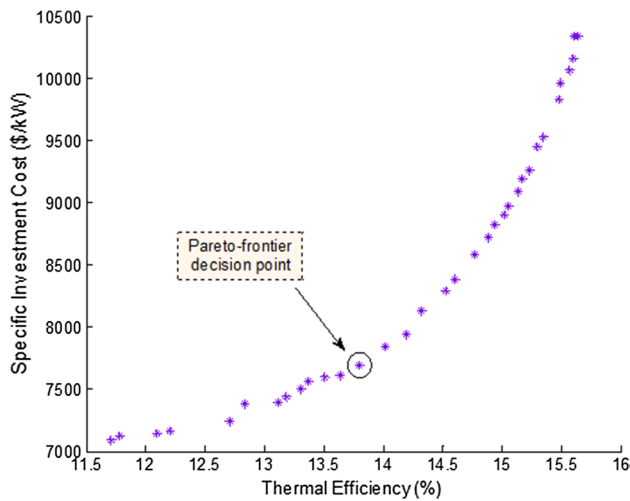


**Fig. 9** Pareto optima for R-601

When recuperation is done the four dry organic working fluids show almost similar thermodynamic behaviour as thermal efficiency differs by only 1.02%. With respect to thermal efficiency point of view R-601 is the most efficient (13.78%) and on the contrary R-236ea is the least efficient (12.78%). SIC has extreme values of 7439.24 \$/kW for R-236ea and 8057.38 \$/kW for R-123.

Results indicate that the organic compound which is most economical is not most efficient thermodynamically. R-601 is decided to be the most suitable candidate for such system as it gives the lowest value of ratio of SIC to thermal efficiency.

A comparison between two architectures i.e. BORC and RORC systems has also been done by picking results of

four dry organic compounds from BORC system. Table 10 presents this comparison in the form of percentage increase or decrease in objective functions with the use of recuperation in BORC system.

It is found that for all organic fluids addition of recuperator results in increase of thermal efficiency as well as SIC of the system. Net useful power output does remain same in both architectures of the system because of identical implemented conditions. The heat duty of evaporator is decreased by the inclusion of an internal heat exchanger (recuperator) which uplifts the thermal efficiency but SIC rises more significantly. Although required area for preheating in evaporator gets reduced due to less amount of heat to be transferred but on the other hand installing a recuperator requires large heat transfer area due to lower log mean temperature difference across high pressure and low pressure sides of working fluid. The SIC rise nonetheless dominates the thermal efficiency betterment. If recuperation is required, R-601 can give better thermal efficiency and R-236ea will give minimum SIC rise.

**5.2 Sensitivity analyses**

Sensitivity analysis is performed for BORC system by taking R-21 (best thermal efficiency), R-245ca (best SIC) and R-601 (best value of the ratio of SIC to thermal efficiency).

Figure 10a shows that as the evaporation pressure ( $P_{evap}$ ) increases the thermal efficiency ( $\eta_{th}$ ) also increases governed by two variables net power output and heat transfer in the evaporator. There is one critical value of evaporation pressure which differentiates the behaviour of governing variables.

**Table 9** Decision points obtained after a trade-off for RORC

Organic fluid	Objective functions		Tradeoff SIC/ $\eta_{th}$	Decision variables				Net power
	$\eta_{th}$ (%)	SIC (\$/kW)		$P_{evap}$ (kPa)	Superheat (°C)	PPTD <sub>evap</sub> (°C)	PPTD <sub>cond</sub> (°C)	
R-123	13.4409	8057.38	599.47	970.68	0.9632	6.4314	14.5525	207.44
R-236ea	12.7763	7439.24	582.27	2020.70	0.4872	6.4002	14.5325	237.30
R-245ca	13.2699	7537.14	567.99	1136.19	0.2667	6.5214	14.7517	218.86
R-601	13.7987	7697.04	557.81	720.27	0.4578	6.4306	13.7152	211.02

**Table 10** Comparison of BORC with RORC

Organic fluid	Thermal efficiency (%)			SIC (\$/kW)		
	BORC	RORC	% Increase	BORC	RORC	% Increase
R-123	12.3744	13.4409	8.06	6374.03	8057.38	26.40
R-236ea	11.4180	12.7763	12.28	6068.80	7439.24	22.57
R-245ca	12.0994	13.2699	9.92	6063.91	7537.14	24.29
R-601	12.2368	13.7987	13.11	6071.83	7697.04	26.76

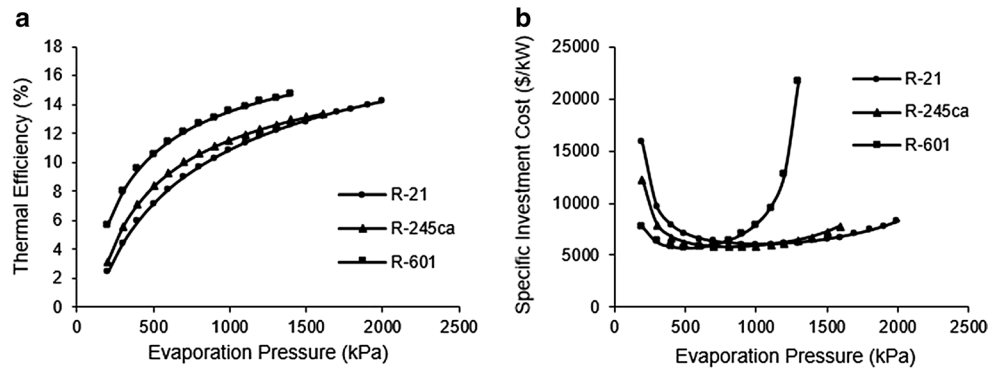


**Fig. 10** a Sensitivity analysis of variation between  $P_{\text{evap}}$  and  $\eta_{\text{th}}$ . b Sensitivity analysis of variation between  $P_{\text{evap}}$  and SIC

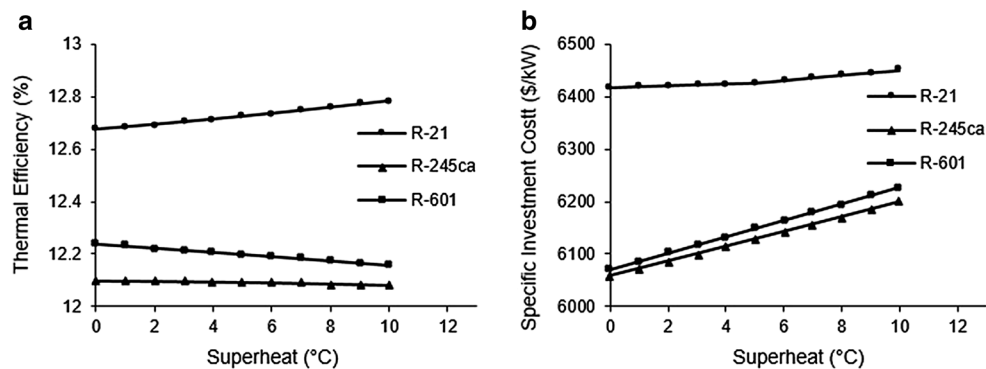


**Fig. 11** a Sensitivity analysis of variation between superheat and  $\eta_{\text{th}}$ . b Sensitivity analysis of variation between superheat and SIC

Up to this value net power output increases after which it declines. The heat intake in evaporator constantly decreases. Prior to the critical value rise of net power and fall of heat given lead to increase in thermal efficiency but after passing this value power output fall is lesser in magnitude compared to heat supplied fall which keeps thermal efficiency rising but at slower pace. SIC depends upon net power output and cost. Up to critical value of evaporation pressure, net power and specific cost increases but afterwards both start decreasing. Actually beyond that point enhancement of evaporation pressure leads the total cost to decrease at a higher rate than the net power output hence SIC increases (see Fig. 10b).

The superheating before turbine inlet does not exert persuasive influence over thermal efficiency. Results conclude that thermal efficiency is affected only by 0.95% increase when superheat is raised from 0 to 10 °C for R-21. Corresponding change for R-245ca and R-601 is 0.14 and 0.65% decrease. R-21 being wet fluid gets increase in thermal efficiency while converse behaviour is exhibited by dry fluids. Increase in superheat decreases the net power output as well as heat taken by working fluid in the evaporator for all fluids. For R-21 reduction of net power output dominates the heat gained reduction

giving positive slope of curve while for R-245ca and R-601 net power output fall is dominated by heat reduction in evaporator giving negative slope of the curves as shown in Fig. 11a. Figure 11b implies that superheating at turbine inlet has direct effect on SIC. Superheating decreases the area of evaporator demanded by lesser amount of heat because of reduced mass flow rate of fluid thus decreasing the total cost which surpasses the fall in net power output eventually yielding an increase in SIC.

Pinch point temperature difference across evaporator ( $PPTD_{\text{evap}}$ ) and condenser ( $PPTD_{\text{cond}}$ ) has no effect on thermal efficiency. This is because both temperature differences are set to be independently determining the heat source and sink sides' temperatures. Furthermore, as heat source mass flow rate is independently fixed the working fluid's mass flow rate gets decreased after increasing the  $PPTD_{\text{evap}}$  causing reduction in net power output and heat transfer in evaporator in equal proportion (as in Fig. 12a).

Changing  $PPTD_{\text{cond}}$  has no effect on either parameter governing thermal efficiency (Fig. 13a).  $PPTD_{\text{evap}}$  needs to be lesser for economical design of ORC systems. Higher the  $PPTD_{\text{evap}}$  lower is the net power output because of lower mass flow rate of refrigerant required.



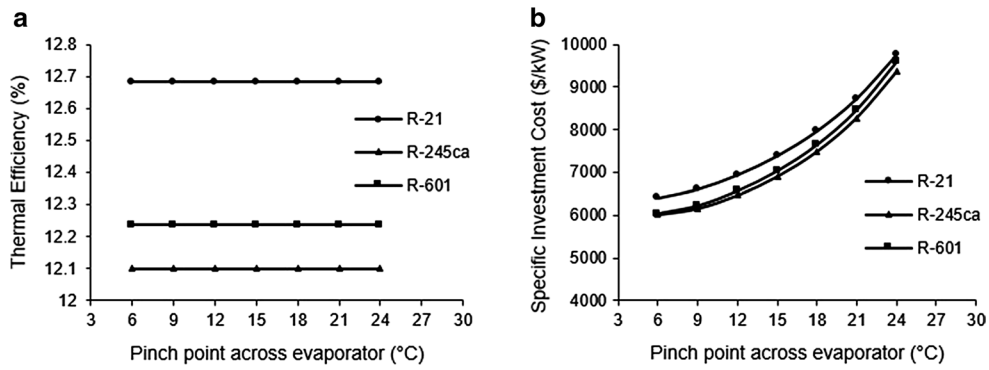


**Fig. 12** a Sensitivity analysis of variation between  $PPTD_{evap}$  and  $\eta_{th}$ . b Sensitivity analysis of variation between  $PPTD_{evap}$  and SIC

**Fig. 13** a Sensitivity analysis of variation between  $PPTD_{cond}$  and  $\eta_{th}$ . b Sensitivity analysis of variation between  $PPTD_{cond}$  and SIC

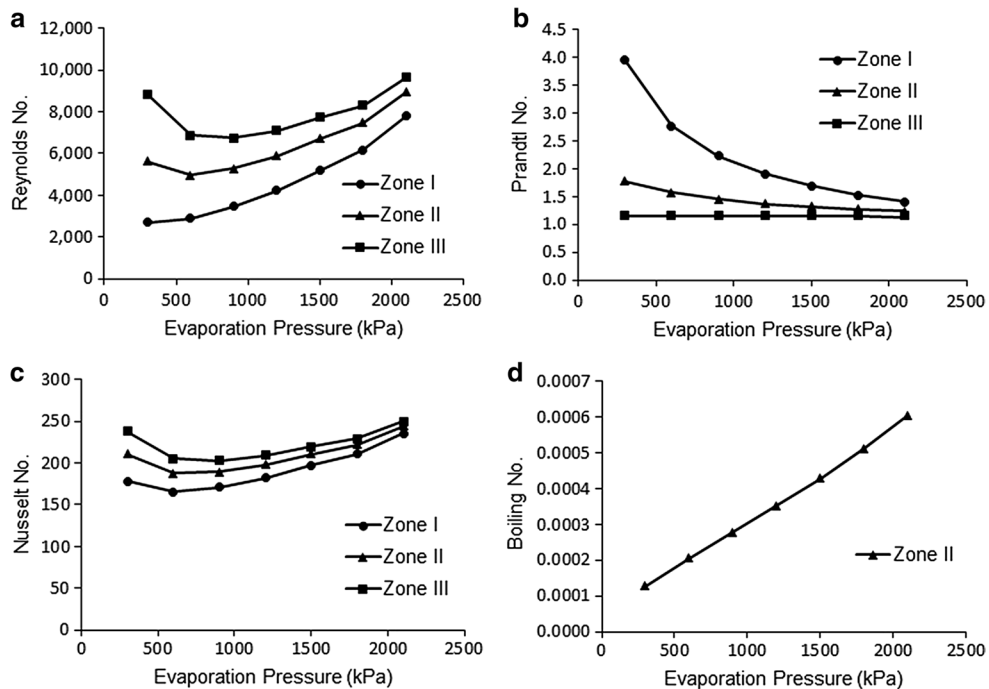
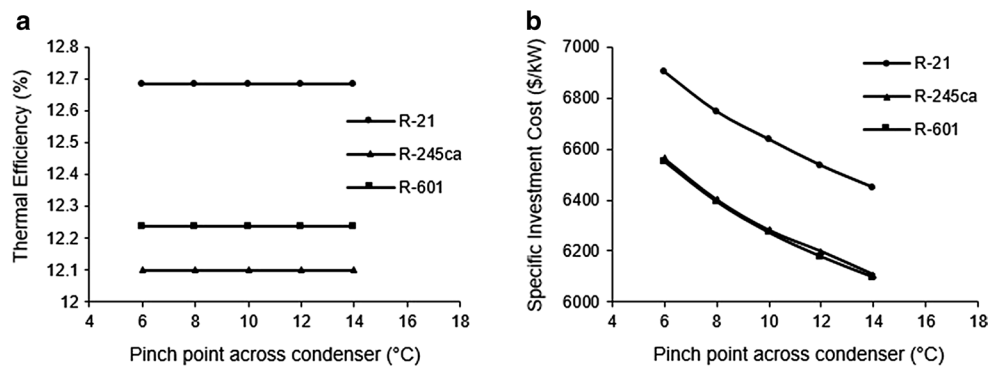


**Fig. 14** a Sensitivity analysis of variation between  $P_{evap}$  and Re No. b Sensitivity analysis of variation between  $P_{evap}$  and Pr No. c Sensitivity analysis of variation between  $P_{evap}$  and Nu No. d Sensitivity analysis of variation between  $P_{evap}$  and Bo No.

Total cost of ORC systems also decreases as a result of reduced turbine and pump works and area required for heat transfer. The decrease of net power output is dominant that leads to increase in SIC as depicted in Fig. 12b. Larger  $PPTD_{cond}$  tends to decrease the SIC (see Fig. 13b).

The sensitivity analysis of dimensionless numbers ( $Re$ ,  $Nu$ ,  $Pr$  and  $Bo$  Nos.) with change in decision variables has also been performed. In Fig. 14a–d the results of variation with respect to evaporation pressure ( $P_{evap}$ ) are shown for R-21 for heat source side. For cooling water side and superheat, a steady and straight line pattern is observed for all dimensionless numbers. With the increase in  $P_{evap}$  an increase in Reynolds No. is observed in heat source side in contrast to refrigerant side where first Reynolds No. decreases and then behaves linearly. In Prandtl No. no major variation is observed in both heat source and refrigerant sides. Similarly, Nusselt No. shows no noticeable variation in the investigated range. Boiling No. increases at constant rate within this range.

### 5.3 Net present value (NPV) and electricity production cost (EPC)

Based on the results of dual-objective optimization (Tables 8, 9, 10), R-601 is selected for estimating economic performance of both systems based on net present value method. Given the assumed economic factors and indices in Table 4, the CRF comes out to be ranged between 0.0672 and 0.1424. The annuity may vary from 84,562.95 to 179,122.74 and 109,173.73 to 231,253.72 \$/year for BORC

and RORC respectively. There is 29.1% increase in annuity for RORC. This is because of significant rise in specific investment cost with nearly same net power output and therefore corresponding rise in total investment cost due to added internal heat exchanger as recuperator.

Net present value (NPV) and electricity production cost (EPC) for two options are shown in Table 11. For 20 years of plant lifetime both BORC and RORC are feasible with any interest rate, however for RORC due to higher TIC, operation and maintenance costs, NPV is lower as compared to BORC. A higher value of EPC is observed for RORC with less gain as compared to BORC.

## 6 Conclusions

Seven different organic compounds were preferably selected and employed to discuss the thermo-economic behaviour of two architectures of ORC systems. The key features of the research work include creation of numerical simulation model in MATLAB program and use of NSGA-II as a dual-objective optimization method in genetic algorithm for procuring pareto optimal solutions. The work is concluded as follows:

- Both architectures of ORC systems give a net power output ranging from 201 to 243 kW for different organic compounds under defined simulation conditions. None of the compounds is best at the same time for satisfying two conflicting objectives.

**Table 11** Comparison of economic performance indicators for R-601 (unit price of electricity = 0.12 \$/kWh)

System		BORC			RORC		
SIC (\$/kW)		6071.83			7697.04		
$W_{net}$ (kW)		207.2			211.02		
TIC = SIC. $W_{net}$ (\$)		1,258,083.17			1,624,229.38		
Indicators		i (%)					
	n (years)	3	5	7	3	5	7
NPV (\$)	10	155,556	21,575	−94124 <sup>a</sup>	−232,798 <sup>a</sup>	−364,674 <sup>a</sup>	−478,555 <sup>a</sup>
	15	720,291	462,051	251,295	323,065	68,882	−138,563 <sup>a</sup>
	20	1,207,436	807,175	497,574	802,558	408,584	103,847
PP (years)		9	10	12	13	15	18
EPC (\$/kWh)	10	0.1083	0.1182	0.1286	0.1372	0.1498	0.1631
	15	0.0812	0.0914	0.1022	0.1029	0.1158	0.1296
	20	0.0678	0.0783	0.0898	0.0859	0.0993	0.1138
G (\$/kWh)	10	0.0117	0.0018	−0.0086 <sup>a</sup>	−0.0172 <sup>a</sup>	−0.0298 <sup>a</sup>	−0.0431 <sup>a</sup>
	15	0.0388	0.0286	0.0178	0.0171	0.0042	−0.0096 <sup>a</sup>
	20	0.0522	0.0417	0.0302	0.0341	0.0207	0.0062

<sup>a</sup> Infeasible option

- For BORC, R-21 is a strong candidate if higher thermal efficiency is needed whereas R-245ca is a strong candidate if SIC is preferable objective function. Comparable behaviour is noted for R-601 as it loses merely 0.446% thermal efficiency than that of R-21 but gains 346.41 \$/kW benefit which makes it third suitable option. R-1234ze is found to be the weakest candidate on any ground.
- For RORC, R-601 outperforms thermodynamically while R-236ea does it cost wise.
- Addition of recuperator improves thermal efficiency at an average of 10.84% for four dry organic compounds. Corresponding significant rise in SIC is 25% on the average.
- Out of all decision variables evaporation pressure significantly affects the objective functions. Each working fluid has its own critical value of evaporation pressure where it gives higher thermal efficiency together with lowest SIC.
- Superheat optimal value is close to its lower boundary value (<1 °C) and it is pointed out that thermal efficiency is not effectively increased rather there is increase in SIC as a whole if superheat is raised therefore genetic algorithm evolves towards lower bound of superheat.
- The optimal pinch point is located at upper bound for condenser and lower bound for evaporator. The pinch point temperature difference across any heat exchanger does not affect thermal efficiency of the system at all.
- Evaporator pinch point fall and condenser pinch point rise lead to economically optimal system design.
- Economic analyses show that both (BORC and RORC) are economically feasible however RORC, due to higher total investment cost (TIC) and operation & maintenance costs, has lower net present value and higher pay-back period as compared to BORC.

## References

1. Quoilin S, Lemort V (2011) The organic rankine cycle: thermodynamics, applications and optimization. In: Exergy, energy system analysis, and optimization. UNESCO-EOLSS
2. Maizza V, Maizza A (2001) Unconventional working fluids in organic Rankine-cycles for waste energy recovery systems. *Appl Therm Eng* 21(3):381–390
3. Ziviani D, Beyene A, Venturini M (2014) Advances and challenges in ORC systems modeling for low grade thermal energy recovery. *Appl Energy* 121:79–95
4. Chen H, Goswami DY, Stefanakos EK (2010) A review of thermodynamic cycles and working fluids for the conversion of low-grade heat. *Renew Sustain Energy Rev* 14(9):3059–3067
5. Walraven D, Laenen B, D'haeseleer W (2014) Comparison of shell-and-tube with plate heat exchangers for the use in low-temperature organic Rankine cycles. *Energy Convers Manag* 87:227–237
6. Jin ZH, Park GT, Lee YH, Choi S, Chung H, Jeong H (2008) Design and performance of pressure drop and flow distribution to the channel in plate heat exchanger. In: *Eng Opt – International Conference on Engineering Optimization*, Rio de Janeiro, Brazil, 01–05 June 2008
7. Wang L, Sunden B (2003) Optimal design of plate heat exchangers with and without pressure drop specifications. *Appl Therm Eng* 23(3):295–311
8. Stijepovic MZ, Linke P, Papadopoulos AI, Grujic AS (2012) On the role of working fluid properties in Organic Rankine Cycle performance. *Appl Therm Eng* 36:406–413
9. Hung T-C (2001) Waste heat recovery of organic Rankine cycle using dry fluids. *Energy Convers Manag* 42(5):539–553
10. Kosmadakis G, Manolakos D, Kyritsis S, Papadakis G (2009) Economic assessment of a two-stage solar organic Rankine cycle for reverse osmosis desalination. *Renew Energy* 34(6):1579–1586
11. Meinel D, Wieland C, Spliethoff H (2014) Economic comparison of ORC (organic Rankine cycle) processes at different scales. *Energy* 74:694–706
12. Atrens AD, Gurgenci H, Rudolph V (2011) Economic optimization of a CO<sub>2</sub>-based EGS power plant. *Energy Fuels* 25(8):3765–3775
13. Quoilin S, Van Den Broek M, Declaye S, Dewallef P, Lemort V (2013) Techno-economic survey of organic Rankine cycle (ORC) systems. *Renew Sustain Energy Rev* 22:168–186
14. Li M, Wang J, Li S, Wang X, He W, Dai Y (2014) Thermo-economic analysis and comparison of a CO<sub>2</sub> transcritical power cycle and an organic Rankine cycle. *Geothermics* 50:101–111
15. Calise F, Capuozzo C, Carotenuto A, Vanoli L (2014) Thermo-economic analysis and off-design performance of an organic Rankine cycle powered by medium-temperature heat sources. *Sol Energy* 103:595–609
16. Lecompte S, Lemmens S, Verbruggen A, van den Broek M, De Paepe M (2014) Thermo-economic comparison of advanced organic Rankine cycles. *Energy Procedia* 61:71–74
17. Quoilin S, Declaye S, Tchanche BF, Lemort V (2011) Thermo-economic optimization of waste heat recovery organic Rankine cycles. *Appl Therm Eng* 31(14):2885–2893
18. Pierobon L, Nguyen T-V, Larsen U, Haglind F, Elmegaard B (2013) Multi-objective optimization of organic Rankine cycles for waste heat recovery: application in an offshore platform. *Energy* 58:538–549
19. Imran M, Usman M, Park B-S, Kim H-J, Lee D-H (2015) Multi-objective optimization of evaporator of organic Rankine cycle (ORC) for low temperature geothermal heat source. *Appl Therm Eng* 80:1–9
20. Wang J, Yan Z, Wang M, Li M, Dai Y (2013) Multi-objective optimization of an organic Rankine cycle (ORC) for low grade waste heat recovery using evolutionary algorithm. *Energy Convers Manag* 71:146–158
21. Sanaye S, Hajabdollahi H (2010) Thermal-economic multi-objective optimization of plate fin heat exchanger using genetic algorithm. *Appl Energy* 87(6):1893–1902
22. Ahmadi P, Dincer I, Rosen MA (2013) Thermodynamic modeling and multi-objective evolutionary-based optimization of a new multigeneration energy system. *Energy Convers Manag* 76:282–300
23. Ayub ZH (2003) Plate heat exchanger literature survey and new heat transfer and pressure drop correlations for refrigerant evaporators. *Heat Transf Eng* 24(5):3–16
24. García-Cascales J, Vera-García F, Corberán-Salvador J, González-Maciá J (2007) Assessment of boiling and condensation heat transfer correlations in the modelling of plate heat exchangers. *Int J Refrig* 30(6):1029–1041

25. Hsieh Y, Lin T (2002) Saturated flow boiling heat transfer and pressure drop of refrigerant R-410A in a vertical plate heat exchanger. *Int J Heat Mass Transf* 45(5):1033–1044
26. Han D-H, Lee K-J, Kim Y-H (2003) The characteristics of condensation in brazed plate heat exchangers with different chevron angles. *J Korean Phys Soc* 43(1):66–73
27. Han D-H, Lee K-J, Kim Y-H (2003) Experiments on the characteristics of evaporation of R410A in brazed plate heat exchangers with different geometric configurations. *Appl Therm Eng* 23(10):1209–1225
28. Lecompte S, Huisseune H, van den Broek M, Vanslambrouck B, De Paepe M (2015) Review of organic Rankine cycle (ORC) architectures for waste heat recovery. *Renew Sustain Energy Rev* 47:448–461
29. Roy J, Misra A (2012) Parametric optimization and performance analysis of a regenerative organic Rankine cycle using R-123 for waste heat recovery. *Energy* 39(1):227–235
30. Imran M, Park BS, Kim HJ, Lee DH, Usman M, Heo M (2014) Thermo-economic optimization of regenerative organic Rankine cycle for waste heat recovery applications. *Energy Convers Manag* 87:107–118
31. Maraver D, Royo J, Lemort V, Quoilin S (2014) Systematic optimization of subcritical and transcritical organic Rankine cycles (ORCs) constrained by technical parameters in multiple applications. *Appl Energy* 117:11–29
32. Brasz LJ, Bilbow WM (2004) Ranking of working fluids for organic Rankine cycle applications. In: *International Refrigeration and Air Conditioning Conference*, Purdue, IN, USA, 12–15 July 2004
33. Wang E, Zhang H, Fan B, Ouyang M, Zhao Y, Mu Q (2011) Study of working fluid selection of organic Rankine cycle (ORC) for engine waste heat recovery. *Energy* 36(5):3406–3418
34. Quoilin S, Declaye S, Legros A, Guillaume L, Lemort V (2012) Working fluid selection and operating maps for organic Rankine cycle expansion machines. In: *Proceedings of the 21st international compressor conference at Purdue*, p 10
35. Xi H, Li M-J, Xu C, He Y-L (2013) Parametric optimization of regenerative organic Rankine cycle (ORC) for low grade waste heat recovery using genetic algorithm. *Energy* 58:473–482
36. Rashidi M, Galanis N, Nazari F, Parsa AB, Shamekhi L (2011) Parametric analysis and optimization of regenerative Clausius and organic Rankine cycles with two feedwater heaters using artificial bees colony and artificial neural network. *Energy* 36(9):5728–5740
37. Mago PJ, Chamra LM, Srinivasan K, Somayaji C (2008) An examination of regenerative organic Rankine cycles using dry fluids. *Appl Therm Eng* 28(8):998–1007
38. Hajabdollahi H, Ganjehkaviri A, Jaafar MNM (2015) Thermo-economic optimization of RSORC (regenerative solar organic Rankine cycle) considering hourly analysis. *Energy* 87:369–380
39. Wang J, Zhao L, Wang X (2012) An experimental study on the recuperative low temperature solar Rankine cycle using R245fa. *Appl Energy* 94:34–40
40. Ventura C, Rowlands AS (2015) Recuperated power cycle analysis model: investigation and optimisation of low-to-moderate resource temperature Organic Rankine Cycles. *Energy* 93:484–494
41. Ge Z, Wang H, Wang H-T, Wang J-J, Li M, Wu F-Z, Zhang S-Y (2015) Main parameters optimization of regenerative organic Rankine cycle driven by low-temperature flue gas waste heat. *Energy* 93:1886–1895
42. Li M, Wang J, He W, Gao L, Wang B, Ma S, Dai Y (2013) Construction and preliminary test of a low-temperature regenerative organic Rankine cycle (ORC) using R123. *Renew Energy* 57:216–222
43. Feng Y, Zhang Y, Li B, Yang J, Shi Y (2015) Comparison between regenerative organic Rankine cycle (RORC) and basic organic Rankine cycle (BORC) based on thermoeconomic multi-objective optimization considering exergy efficiency and levelized energy cost (LEC). *Energy Convers Manag* 96:58–71
44. Jung H, Krumdieck S (2014) Modelling of organic Rankine cycle system and heat exchanger components. *Int J Sustain Energy* 33(3):704–721
45. Yu G, Shu G, Tian H, Wei H, Liang X (2016) Multi-approach evaluations of a cascade-organic Rankine cycle (C-ORC) system driven by diesel engine waste heat: Part B-techno-economic evaluations. *Energy Convers Manag* 108:596–608
46. de Oliveira NR, Sotomonte CAR, Coronado CJ, Nascimento MA (2016) Technical and economic analyses of waste heat energy recovery from internal combustion engines by the organic Rankine cycle. *Energy Convers Manag* 129:168–179
47. Kosmadakis G, Manolakos D, Papadakis G (2011) Simulation and economic analysis of a CPV/thermal system coupled with an organic Rankine cycle for increased power generation. *Sol Energy* 85(2):308–324